

High tunnel magnetoresistance in epitaxial Fe/MgO/Fe tunnel junctions

J. Faure-Vincent,^{a)} C. Tiusan, E. Jouguelet, F. Canet, M. Sajieddine, C. Bellouard, E. Popova, M. Hehn, F. Montaigne, and A. Schuhl

Laboratoire de Physique des Matériaux, BP 239, 54506 Vandoeuvre lès Nancy, France

(Received 10 March 2003; accepted 23 April 2003)

We report on spin-polarized tunneling in fully epitaxial Fe/MgO/Fe/Co tunnel junctions. By increasing the thickness of the insulating layer (t_{MgO}), we have strongly enhanced the tunnel magnetoresistance. Values up to $\sim 100\%$ at 80 K ($\sim 67\%$ at room temperature) have been observed with $t_{\text{MgO}}=2.5$ nm. This tunnel magnetoresistance ratio, which is much larger than the one predicted by the Jullière's model, can be understood in the framework of *ab initio* calculations.

© 2003 American Institute of Physics. [DOI: 10.1063/1.1586785]

The tunnel magnetoresistance effect (TMR) in magnetic tunnel junctions (MTJs) is widely studied nowadays due to the large-scale potential applications of MTJs in sensors and data storage devices: i.e., magnetic random-access memories and read heads.¹ Up until now, the most frequently elaborated MTJs contain polycrystalline or amorphous insulating barriers, essentially Al_2O_3 . With this insulating material, 10% of TMR have been reached at room temperature (RT) in 1995.² By optimizing the alumina barrier growth conditions, they typically show TMR ratios at RT ranging up to 40%–50%.³ Such magnitude for the TMR remains in agreement with the simple Jullière's model which involves only the spin polarization of the ferromagnetic electrodes.

Recently, *ab initio* calculations^{4,5} predicted large TMR ratios in single crystalline MTJs, namely Fe/MgO/Fe. They are driven by the different tunneling mechanisms for the majority and minority spin channels in single crystal junctions. The symmetry of the Bloch states at the Fermi level and the symmetry-related decay of the evanescent states in the barrier layer are different for the majority and the minority electrons and so the TMR is predicted to increase with increasing insulating layer thickness. Moreover, the tunneling conductivity is affected by the interfacial effects. Scattering and/or resonance effects modulate the interfacial wave function matching and therefore the tunneling probability. Following the theoretical calculations, in the Fe/MgO/Fe MTJs, the TMR is supposed to increase when increasing the MgO thickness, and then to reach a maximum value above 1000% for about 10 atomic planes of MgO.^{4,5}

Experimentally, the epitaxial growth of Fe/MgO/Fe system is well controlled,⁶ and several studies have already been performed. For example, a TMR ratio of 27% at RT has been observed in Fe/MgO/Fe₅₀Co₅₀ (Ref. 7) by using laser ablation crystal growth. In our previous work,⁸ we have reported 17% at RT, in this letter, we show that, as predicted by *ab initio* calculations,^{4,5} a TMR ratio well above the limit of the Jullière's model can be achieved by increasing the thickness of the barrier from 1.0 to 2.5 nm.

The Fe/MgO/Fe/Co multilayer is grown by molecular-beam epitaxy (MBE). Details about the procedure and on the crystalline quality of the sample can be found elsewhere.⁸

Briefly, after annealing the MgO substrate at 500 °C for 20 min, a first 50 nm thick Fe layer is deposited at RT using a Knudsen cell, then annealed at 450 °C for 15 min in order to smooth its surface. The MgO insulating layer is subsequently deposited at RT using an electron gun. We observe a two-dimensional layer-by-layer growth of MgO up to 10 to 15 monolayers asserted by reflection high-energy electron diffraction (RHEED) intensity oscillations and oscillations of the in-plane lattice parameter. The observation of clear RHEED intensity oscillations ensures us to have high-quality ultrathin layers. The second magnetic electrode is a bilayer composed of a 5 nm thick Fe layer, epitaxially grown on the top of the MgO barrier and magnetically hardened by a 50 nm thick Co layer. Finally, we cap the sample with a 10 nm Au layer providing large conductivity and preventing *ex situ* oxidation. The continuity of the insulating MgO layer has been previously checked down to 0.8 nm thickness, at different spatial scales in our previous study.⁸

After the MBE growth of the multilayer stack, the MTJ structures are patterned by UV lithography and Ar ion etching, step-by-step controlled *in situ* by Auger spectroscopy. First, the top of the junction is defined by digging the upper junction electrode just below the insulating layer. Subsequently, the physical separation of all the junctions and the bottom electrode definition is done. Furthermore, the individual junctions are protected by an insulating SiO_2 layer deposited by radio-frequency reactive sputtering, then the bottom electric contact is accessed by a subsequent lithography/ion milling step. Finally, macroscopic contacts are defined successively by lithography, deposition of a conducting Al thick layer, and lift-off technique.

The magnetic properties are controlled by the four-fold anisotropy of the layers, related to their epitaxial growth. For low MgO thickness (less than 0.8 nm), the magnetization curves $M(H)$ performed on the multilayer stack of the junction with variable MgO thicknesses have emphasized a strong antiferromagnetic coupling related to an interlayer exchange coupling by spin-polarized tunneling.⁹ This coupling vanishes for larger MgO thickness. Above 1 nm, the residual coupling field is only related to orange peel coupling, being of the order of few Oe. In this regime, along the easy axis, we obtain square magnetization curves with a large field range between the reversal of the soft (coercive field <40

^{a)}Electronic mail: faure@lpm.u-nancy.fr

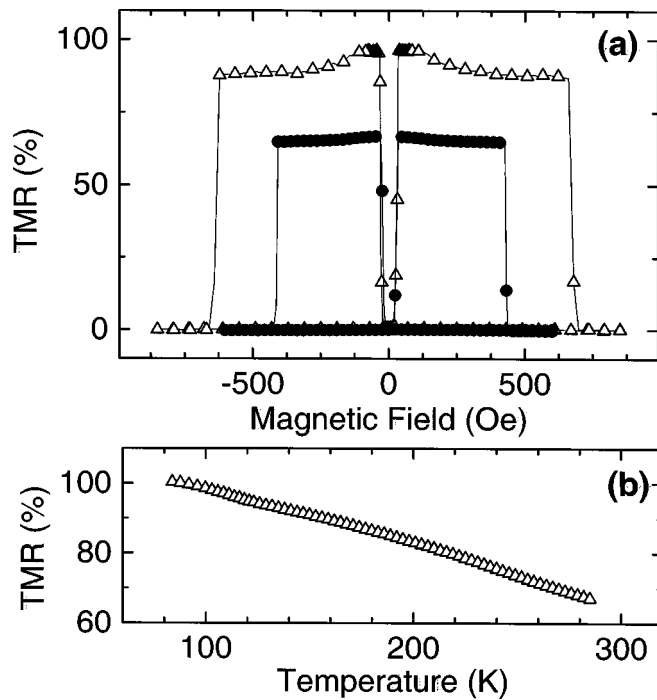


FIG. 1. (a) TMR of a $65 \times 95 \mu\text{m}^2$ large MgO (100)/Fe/MgO-2.5 nm/Fe/Co/Au junction at 80 K ($-\Delta-$) and 293 K ($-\bullet-$). The measurements are performed along the easy axis, the junction being biased at 10 mV. (b) Variation of TMR at 10 mV with temperature.

Oe) and the hard (coercive field >400 Oe) magnetic layers of the junction, respectively.

The transport properties presented in this letter are measured on a typical $65 \times 95 \mu\text{m}^2$ junction with a nominal 2.5 nm thick MgO tunnel barrier. All of the transport measurements have been performed in a two-contact mode at constant applied voltage with an applied field along the easy axis (i.e., $\parallel [100]\text{Fe}$). The Fe bottom electrode has been connected to the positive bias voltage.

Figure 1 shows typical resistance versus field $R(H)$ cycles taken at low temperature (LT=80 K) and room temperature (RT=293 K) for an applied voltage of +10 mV. From the positive saturation field, as the applied magnetic field decreases and reverses its sign, around 40 Oe, one can notice a very sharp augmentation of the resistance according to the magnetization reversal of the soft layer from the parallel (P) to an antiparallel (AP) configuration with respect to the top magnetic moment. The AP state is preserved in a large field range.

At the end of this plateau, the low resistance P state is reached again when the hard layer magnetization reverses abruptly. Note that at LT, as expected, the coercive field of the hard layer is enhanced from about 400 to 600 Oe.

The resistance measured between the top and the bottom of the junction contact pad is 126Ω (72Ω) in the P state and 253Ω (120Ω) in the AP state at LT (RT), with a good reproducibility over the junctions on the same substrate. This values have been corrected by subtracting the electrode/access resistance (typically 10Ω). Therefore, the TMR ratio, calculated as $\text{TMR} = (R_{\text{AP}} - R_{\text{P}}) / R_{\text{P}}$ is about 100% at LT and 67% at RT, respectively.

Indeed, we have carefully checked the occurrence of any geometrical effects. By taking into account the junction re-

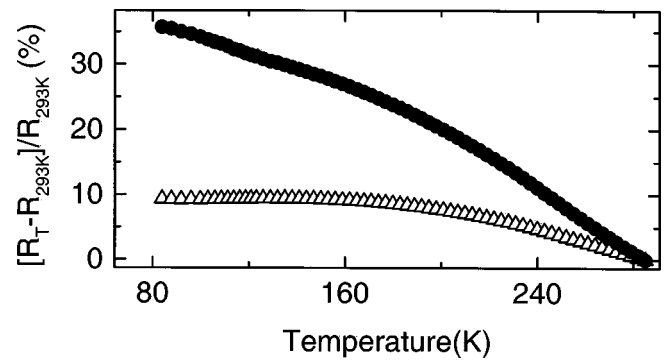


FIG. 2. Relative variations of the junction resistance at 10 mV in the P ($-\Delta-$) and AP ($-\bullet-$) states as a function of temperature.

sistance and the square resistance of the electrodes, the typical length scale of current distribution in our system was estimated¹⁰ to about $600 \times 600 \mu\text{m}^2$, much larger than our junction area. Consequently, in our samples, we can neglect current distributions effects. Moreover, the transport measurements presented here have been performed in the two-contact configuration where, in any case, the TMR would be underestimated by current distribution effects, contrary to four-contact measurements where it could be overestimated.¹⁰

The temperature dependence of the tunnel junction resistance is shown in Fig. 2 in the P and AP states. As expected for the tunneling transport, the resistance increases by decreasing the temperature from RT to LT. However, as we can observe from our measurements, the temperature dependence of the resistance is more pronounced for the AP state (35% of relative variation) with respect to the P one (only 10% of relative variation). This can be explained, as predicted theoretically, by the strong temperature dependence of the scattering driven interfacial contributions in the spin-polarized tunneling of the minority spin channel. The transport in the P state is dominated by the majority spin channel whose conduction mechanism is related to pure tunneling which is less temperature dependent. Therefore, the enhancement of the TMR ratio at LTs from about 67% at RT to about 100% at LT (Fig. 1), is driven by the temperature dependence of the minority spin channel transport mechanisms reflected in the variation of the R_{AP} with the temperature.

The positive and negative branches of both static [current-voltage (I/V)] and dynamic (dI/dV) conductivity at RT in the saturated state are different (Fig. 3). This asymmetry suggests that the Fe/MgO (bottom) and MgO/Fe (top) interfaces are not similar and, therefore, their electronic structures are different. Indeed, the tunnel current is a probe of the interfacial density of states: When biasing the junction, the electrons injected from the Fermi level in one side of the barrier scan in energy the density of states of the other interface.

We attribute the difference in the electronic structure of the two Fe/MgO interfaces to the different local arrangement of O and Fe atoms. Experimentally, this is directly related to the pollution in oxygen of one barrier interface during the elaboration procedure. As already reported in literature,¹¹ during the evaporation of MgO, the bottom Fe electrode sees the molecular O_2 coming from the recombination of the O on the MBE chamber walls. In our experiments, the presence of

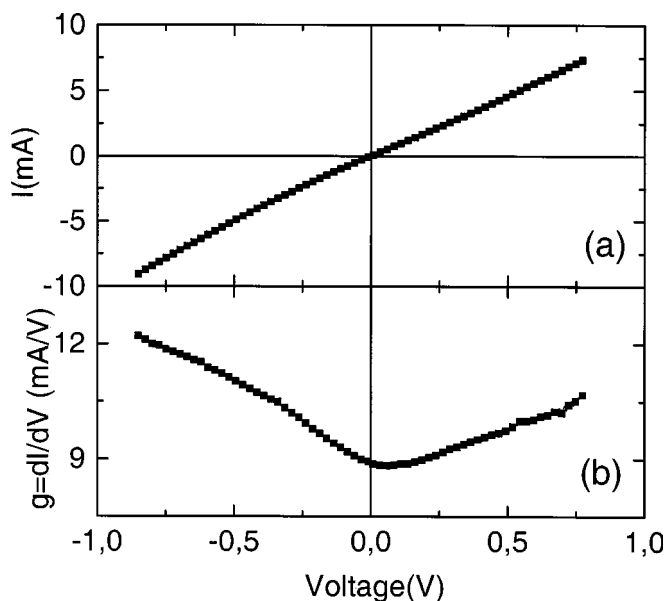


FIG. 3. Typical transport curves (a) static conductivity I - V and (b) dynamic conductivity $g = dI/dV$, at room temperature in the P state for a 2.5 nm thick MgO layer.

the molecular O_2 during the MgO deposition is reflected by the augmentation of the base pressure from 10^{-10} to 10^{-8} Torr and by its characteristic peak detected by a quadrupole spectrometer. Therefore, one can expect an FeO interface layer between the bottom Fe(001) and the MgO barrier and an oxygen-free upper MgO/Fe(001) interface with Fe growing epitaxially on top of the MgO, with a first layer of Fe laying on top of the O.

The different topologies of the two interfaces implicate different Fe/O bonding. This has drastic consequences on the wave function propagation at the two interfaces, reflected also by different work functions of the two ferromagnetic electrodes. Indeed, for the upper MgO/Fe interface, only one layer of Fe contributes to the bonding. One can expect a vertical bonding with the oxygen via the Fe $3d_{z^2}$ and O $2p_z$ orbitals. For the bottom interface, oxygen polluted, the Fe and O are located almost in the same plane.¹¹ Here, the oxygen atoms have significant bonding with both surface and subsurface Fe layers.¹² Horizontal bonding (within the surface plane) is primarily due to the planar orbitals $3d_{xy}$ and $3d_{x^2-y^2}$ of the Fe, and $2p_x$ and $2p_y$ orbitals of oxygen. Vertical bonding of oxygen to subsurface Fe is accomplished through Fe $3d_{z^2}$ and O $2p_z$ orbitals. Moreover, the presence

of a bottom FeO interface drastically changes the interfacial wave function matching at the bottom interface, the Fe work function and, therefore, the tunneling probability. Consequently, it would explain the lower experimental TMR ratio (only 100% at 80 K) with respect to the theoretical prediction of Butler *et al.*⁵

In summary, in this letter, we report a large TMR at RT in Fe/thick MgO/Fe MTJs. In this system, the TMR increases with increasing insulating layer thickness from 17% to 67% at RT and 100% at LT. From the analysis of the temperature dependence of the magnetotransport characteristics, we point out that the spin-polarized transport is governed by complex interfacial band structure aspects. This is in qualitative agreement with theoretical predictions. We have attributed the quantitative discrepancy with models to an asymmetry between the two interfaces of the tunnel barrier. Then, a much higher TMR ratio up to 1000% should be achieved with fully symmetric Fe/MgO/Fe tunnel junctions.

The authors are grateful to M. Alnot and S. Andrieu for stimulating discussions. This work was supported by the "Conseil Régional de Lorraine" and by the EC NANOMEM Program (IST-1999-13741).

- ¹J. M. Daughton, J. Appl. Phys. **81**, 3758 (1997); W. J. Gallagher, J. H. Kaufman, S. S. P. Parkin, and R. E. Scheuerlin, US Patent No. 5,640,343 (1997).
- ²J. S. Moodera, L. R. Kinder, T. M. Wong, and R. Meservey, Phys. Rev. Lett. **74**, 3273 (1995).
- ³J. J. Sun, V. Soares, and P. P. Freitas, Appl. Phys. Lett. **74**, 448 (1999).
- ⁴J. Mathon and A. Umerski, Phys. Rev. B **63**, 220403R (2001).
- ⁵W. H. Butler, X.-G. Zhang, T. C. Schulthess, and J. M. MacLaren, Phys. Rev. B **63**, 054416 (2001).
- ⁶J. L. Vassent, M. Dynna, A. Marty, B. Gilles, and G. Patrat, J. Appl. Phys. **80**, 5727 (1996); T. Urano and T. Kanaji, J. Phys. Soc. Jpn. **57**, 3403 (1988).
- ⁷M. Bowen, V. Cros, F. Petroff, A. Fert, C. Martinez Boubeta, J. L. Costa-Kramer, J. V. Anguita, A. Cebollada, F. Briones, J. M. de Teresa, L. Morrellon, M. R. Ibarra, F. Guell, F. Peiro, and A. Cornet, Appl. Phys. Lett. **79**, 1655 (2001).
- ⁸E. Popova, J. Faure-Vincent, C. Tiusan, C. Bellouard, H. Fischer, M. Hehn, F. Montaigne, M. Alnot, S. Andrieu, A. Schuhl, E. Snoeck, and V. da Costa, Appl. Phys. Lett. **81**, 1035 (2002).
- ⁹J. Faure-Vincent, C. Tiusan, C. Bellouard, E. Popova, M. Hehn, F. Montaigne, and A. Schuhl, Phys. Rev. Lett. **89**, 107206 (2002).
- ¹⁰R. J. M. van de Veerdonk, J. Nowak, R. Meservey, J. S. Moodera, and W. J. M. de Jonge, Appl. Phys. Lett. **71**, 2839 (1997); F. Montaigne, F. Nguyen Van Dau, and A. Schuhl, J. Magn. Mater. **217**, 231 (2000).
- ¹¹H. L. Meyerheim, R. Popescu, J. Kirschner, N. Jedercy, M. Sauvage-Simkin, B. Heinrich, and R. Pinchaux, Phys. Rev. Lett. **87**, 76102 (2001).
- ¹²H. Huang and J. Hemanson, Phys. Rev. B **32**, 6312 (1985).